Geochemical controls on the elemental composition of siderite: Implications for palaeo-environmental reconstructions

Ritwika Sengupta[1*], Nicholas J. Tosca[1], Stuart A. Robinson[1]

[1]Department of Earth Sciences, University of Oxford , South Parks Road, Oxford, OX1 3AN

*Corresponding author: ritwika.sengupta@earth.ox.ac.uk

*Telephone:+44 (0) 7919376071

1 Abstract

The elemental composition of siderite ($FeCO_3$) has been widely used as a palaeo-environmental proxy, and commonly utilised in the diagnosis of marine influences on Phanerozoic coastal wetland sediments. That siderite might reflect marine or freshwater sources is based on the premise that a marine origin should show an enrichment of Ca and/or Mg, while high concentrations of Mn should reflect precipitation from freshwater. However, the main controls on the elemental composition of siderite, and the degree to which siderite composition reflects parent water chemistry, are poorly understood. To address these issues, we conducted siderite nucleation and seeded growth experiments to examine element partitioning at a variety of saturation states and solution compositions (i.e., cation concentrations, pH, and pCO_2). Results indicate a strong preference for Mn uptake over Ca and Mg, even when Mn is present at concentrations far below those of Ca or Mg. This uptake is enhanced at slower growth rates and lower saturation states, which may, in part, reflect surface structural controls on uptake and or a change in the dominant growth mechanism. Ca uptake only occurred during nucleation experiments, while measurable Mg uptake was not observed in experiments conducted at 20˚C, but increased slightly at 55˚C. These results suggest that the chemical composition of siderite does not directly reflect aqueous cation chemistry as previously assumed and is strongly influenced by kinetics rather than equilibrium behaviour. This leads us to conclude that variations in pore water chemistry alone cannot explain the range of Ca and Mg concentrations reported from geological siderites, and that other factors must be considered (such as physical admixtures of multiple carbonate minerals and/or the products of diagenetic recrystallization).

2 Introduction

Siderite ($FeCO_3$) is found in sedimentary rocks throughout geological time, notably as a constituent of Precambrian banded iron formations (BIFs), and in many sandstones, fine-grained siliciclastics, carbonates, and pedogenic nodules spanning the Precambrian and Phanerozoic (Bahrig, 1989; Choi et al., 2003; Johnson et al., 2008; Lim et al., 2004; Ludvigson et al., 1998; Pye et al., 1990; Robinson et al., 2010; Ufnar et al., 2004a, 2004b; Weibel et al., 2016). Of these deposits, early diagenetic siderite spheres (or "sphaerosiderites"), occurring within a range of strata deposited in dominantly non-marine environments (Ludvigson et al., 1998; Ufnar et al., 2004a; Ludvigson et al., 2013), are perhaps among the most studied examples of siderite precipitation of the Phanerozoic.

As sphaerosiderites are thought to grow in wetland soils, they are considered to be important archives of the continental hydrological system by providing a record of the $\delta^{18}O$ of meteoric groundwater (Mozley and Wersin, 1992; Ludvigson et al., 1998; Choi et al., 2003; Ufnar et al., 2004a; Choi and Kim, 2006; Suarez et al., 2009; Robinson et al., 2010; Ludvigson et al., 2013). As a consequence, unravelling the precise nature of pore waters, from which sphaerosiderites precipitated, has persisted as a major research goal. Indeed, the elemental composition of sphaerosiderites has been extensively used to infer freshwater, brackish or marine porewater conditions, in order to identify those samples likely to record a meteoric groundwater signal (Fisher et al., 1998; Choi et al., 2003; Lim et al., 2004; Ufnar et al., 2004a; Ufnar et al., 2004b; Driese et al., 2004; Robinson et al., 2010; Ludvigson et al., 2013; Weibel et al., 2016). For example, based on sedimentological studies of siderite-bearing strata, sphaerosiderites with more extensive Ca and Mg substitution are considered to reflect a marine influence, while higher concentrations of Mn compared to Ca or Mg are commonly interpreted to reflect freshwater conditions (Mozley, 1989; Ludvigson et al., 1998; Driese et al., 2010).

Previous investigations of Phanerozoic sphaerosiderites have therefore implicitly assumed that the elemental composition of siderite should reflect the chemistry of the growth solution (i.e. palaeo pore waters). However, this assumption is not easily reconciled with laboratory syntheses, which

have failed to reproduce the compositional link between siderite and pore water chemistry (Thornber and Nickel, 1976; Carothers et al., 1988; Mortimer et al., 1997; Jimenez-Lopez and Romanek, 2004; Romanek et al., 2009). Previous studies have examined controls on siderite chemical composition particularly in reference to Ca and Mg. However, experimental conditions are typically associated with crystallisation rates that may be orders of magnitude higher than natural settings (Postma, 1980; Pye et al., 1990; Steinmann and Shotyk, 1997). In contrast, chemical controls on Mn uptake in siderite have not been well constrained, particularly for low supersaturation growth conditions. Mn is often a dominant component in siderite, but comparatively little is known about palaeo-environmental factors leading to the common observations of typically Mn-rich siderites (Fisher et al., 1998; Choi et al., 2003; Lim et al., 2004; Weibel et al., 2016). Similarly, the significance of Mg-rich compositions, and associated changes in Ca reported in ancient sphaerosiderites (Mozley and Wersin, 1992; Fisher et al., 1998; Khim et al., 1999; Khim et al., 2000; Choi et al., 2003; Lim et al., 2004), are poorly understood in the context of laboratory experiments (Thornber and Nickel, 1976; Mortimer et al., 1997; Romanek et al., 2009), which have been unable to reproduce natural concentrations of Mg in siderite. Although the latter observation has been intuitively ascribed to the influence of marine waters (Mozley, 1989; Choi et al., 2003; Ufnar et al., 2004a; Choi and Kim, 2006; Suarez et al., 2009; Robinson et al., 2010; Ludvigson et al., 2013; Weibel et al., 2016), the rates and mechanisms of element incorporation during siderite nucleation and growth are not fully understood. Constraining the factors influencing elemental composition of siderite is critical as a means of understanding the growth conditions and assessing the potential of a given sedimentary deposit to yield robust constraints on palaeoclimate.

The goal of this study is to address these issues through an experimental investigation of the controls on the chemical composition of inorganically-precipitated siderite. In particular, our experiments extend to relatively low saturation states and, hence, growth rates which may more closely represent wetland systems in which modern and ancient siderite growth has occurred. We present results from nucleation and growth experiments investigating a range of factors, such as pCO_2, salinity, cation concentration, temperature, and pH. We then discuss, in light of our results,

the principal factors controlling the elemental composition of siderite in natural and synthetic systems. Finally, we review geological processes that may further modify the elemental composition of sphaerosiderite in sedimentary systems, in order to provide a process-based framework to aid in their robust paleo-environmental interpretation.

3 Methods

Two types of siderite precipitation experiments were conducted; homogeneous nucleation (where siderite was spontaneously precipitated directly from solution) and seeded growth (where siderite overgrowths were precipitated on to pre-existing seed material). These two experiment types can be distinguished on the basis of saturation state, which is controlled by concentration of Fe^{2+}, pCO_2 (or total dissolved inorganic carbon, DIC), and pH. The saturation state of siderite can be expressed with the following relation:

$$FeCO_3(siderite) = Fe^{2+} + CO_3^{2-}$$

At solubility equilibrium:

$$K_{sp} = a_{Fe2+} * a_{CO32-} = 10^{-10.24} \text{ (Fosbøl et al., 2010)}$$

Under non-equilibrium conditions the ion activity product (IAP) and siderite saturation (SI) are:

$$IAP = a_{Fe2+} * a_{CO32^-}$$

$$\Omega = IAP/Ksp$$

$$SI = \log_{10}(\Omega)$$

Recent studies of the Fe(II)-carbonate system at ambient temperature (Dideriksen et al., 2015; Jiang and Tosca, 2019) have shown that homogeneous nucleation of Fe(II)-carbonate commonly involves the initial formation of a precursor phase (i.e., amorphous Fe carbonate or AFC) and that its apparent solubility corresponds approximately equal to an SI = 2.6. Thus, we adopt an operational definition for the threshold associated with homogeneous nucleation at this saturation state (Steefel and Van Cappellen, 1990; Van Cappellen, 1991). The conditions dominated by

siderite growth (in the presence of seed material) should therefore lie within a range of SI = 0 to 2.6 (Dideriksen et al., 2015), while at SI>2.6, the homogeneous nucleation process is expected to dominate.

Precipitation experiments were conducted in 500 ml glass and LDPE bottles, covered in aluminium foil to prevent UV photolysis. The bottles were sealed with no headspace in order to achieve a closed system (and to prevent CO_2 degassing). All experiments were conducted in an anoxic glovebox, with 96% N_2 and 4% H_2 atmosphere. Palladium catalysts and anhydrous $CaSO_4$ desiccant ensured the oxygen concentration within the glovebox remained less than 1ppm, and the ambient atmosphere was kept at low relative humidity. All reactant stock solutions were prepared in the anoxic glovebox using 18 M-Ω deionized (DI) water. The water was purged with O_2 free-N_2 gas for 1 hour (Butler et al., 1994) and then left on a stir plate for 30 minutes in the glovebox to allow for the removal of residual oxygen.

Stock solutions prepared beforehand included 1M NaCl and 1M NaOH. 3-(*N*-morpholino)propanesulfonic acid (MOPS) and NaOH were together used to control the pH, while NaCl was used to produce a range of salinities and ionic strengths, approaching values corresponding to natural settings from fresh to marine pore waters. Because MOPS features significant steric hindrance of its acid-base functional groups, it does not exhibit appreciable complexation with transition metals such as Fe^{2+} in solution (Kandegedara and Rorabacher, 1999). After initial preparation (with $FeCl_2$), the 1 M Fe^{2+} stock solution was treated with Fe^0 powder (>99%, Sigma-Aldrich) and HCl (1M) to reach a pH of 2, and left for 24 hours. This treatment reduced any Fe^{3+} in solution introduced from the reagent powder or from residual oxygen, and stabilised the solution. After 24 hours, the solution was passed through a container with a Nd-magnet embedded in the bottom to remove the Fe^0 from solution. 1M $NaHCO_3$ solution, used to supply the carbonate in the reaction, was freshly prepared before each experiment to limit degassing.

Nucleation experiments were conducted at 20˚C (i.e., ambient temperature) and were started upon the delivery of $NaHCO_3$ stock solution with a syringe before being sealed with an opaque bottle cap. After delivery of the Fe stock solution, the experiments were left to run for 24 hours on an orbital

shaker. The resulting precipitate was vacuum filtered in the glovebox and allowed to dry for 48 hours within the glovebox (covered in foil to avoid photo oxidation). The pH of each experiment was measured at the start (after addition of Fe^{2+}) and at the end (before filtration of precipitate). For growth experiments, the procedure was the same as stated above, except a premade pure (verified by X-ray diffraction) siderite seed was added to facilitate growth. The siderite seed (Supplementary Information) was imaged using FEI FEG Scanning Electron Microscope (SEM) at the Department of Earth Sciences, University of Oxford and the specific surface area was found to be $6 m^2/g$ as analysed using BET surface analysis (Micromeritics 3flex) at the Chemistry Research Laboratory, University of Oxford. Growth experiments were left for 25-30 days without stirring but were periodically shaken. Two elevated temperature growth experiments were also conducted at 40˚C and 55˚C respectively, under the same conditions. In these two cases, a stir plate with an integrated hotplate and temperature probe was used. The temperature probe was placed in the solution through the sealed septum placed in the bottle cap.

The conditions explored within these experiments are summarised in Table 1. Fe concentration was kept constant within batches of experiments, while Ca, Mn, and Mg were varied with reference to Fe. The Fe concentration was chosen based on reported pore waters from modern bogs (Postma, 1980; Pye et al., 1990), which vary from 0.2 – 1 mmol/kg with depth. It was necessary to conduct experiments at a higher concentration of Fe than reported from natural waters to produce enough solid precipitate for a range of analyses, and so that time-resolved changes in aqueous concentration could be observed with relatively high precision. The saturation states of our growth experiments are lower than previous experimental studies (Romanek et al., 2009; Thornber and Nickel, 1976).

	Nucleation	**Growth**	**High Temperature**
Cation concentrations	Fe, Mn, Ca: 1-10 mmol/kg Mg: 0.25 - 52 mmol/kg	Fe, Mn, Ca: 0.1-1 mmol/kg Mg: 0.05 - 5 mmol/kg	Fe: 1 mmol/kg Mg: 0.5 mmol/kg
DIC^-	10 mmol/kg	2 - 5 mmol/kg	5 mmol/kg

pH	7 – 9	7 – 8	7.5
Ionic Strength	0.013-0.7	0.013-0.106	0.013
logΩ	2 - 3.6	0.5 - 1.975	2.38 - 2.65
Stirring	Orbital shaker	No	Hot plate with integrated stir plate
Siderite seed	No	Yes	Yes
Temperature	25˚C	25˚C	40˚C and 55˚C

Table 1: Summary of experimental variables employed in this study

Solution samples were taken at the beginning and end of the nucleation experiments, and every 2–4 days during growth experiments (depending on the length of the experiment). The solution samples were immediately acidified with 5% HNO_3 and analysed for major element chemistry using Inductively Coupled Plasma-Optical Emission Spectrometry (ICP-OES) at Scottish Universities Environmental Research Centre (SUERC) and Department of Earth Sciences, UCL. All analysis batches included matrix matched quality control standards. Rates of reactions were calculated by the difference in measured cation concentration (Fe and Mn) over a given time unit, and correcting the saturation state by subtracting DIC and recalculating for the next time step. Precipitates were analysed using a FEI FEG-SEM at Oxford to image the crystalline morphology at high resolution. An EDS detector was used to constrain elemental composition of experimental precipitates. The precipitates were also analysed using a PANalytical Empyrean Series 2 X-ray diffractometer at Oxford, which used a Co Kα source at 40 kV and 40 mA. Samples were prepared in the glovebox on zero-background single crystal silicon substrates and sealed with X-ray transparent Kapton film prior to analysis.

4 Results

4.1 Fe(II)-carbonate precipitation pathways

After removal of Al foil, precipitates were visibly identified in nearly all experiments. Once filtered, the precipitates ranged in colour from greenish-gray to dark brown, as is typical of $FeCO_3$

synthesis (Fosbol et al., 2010). The precipitates were dried at 25˚C and also changed colour when drying, generally becoming darker. Powder X-Ray diffraction analyses confirmed that experimental precipitates were dominated by Fe(II)-carbonate minerals (Supplementary Information). XRD analysis of precipitates formed between pH 7 and 8 show the material to be mostly siderite. Exceptions to this included some of the higher pH experiments (pH 8 to 9) which also produced chukanovite ($Fe_2(OH)_2CO_3$). Precipitate morphology varied from siderite rhombohedra of various forms (~1-4 µm in length) to spherical particles composed of clusters of smaller rhombs (Fig 1). The spheres were on average 10 µm in diameter, while the constituent rhombs comprising the spheres were typically <1 µm along single crystal edges.

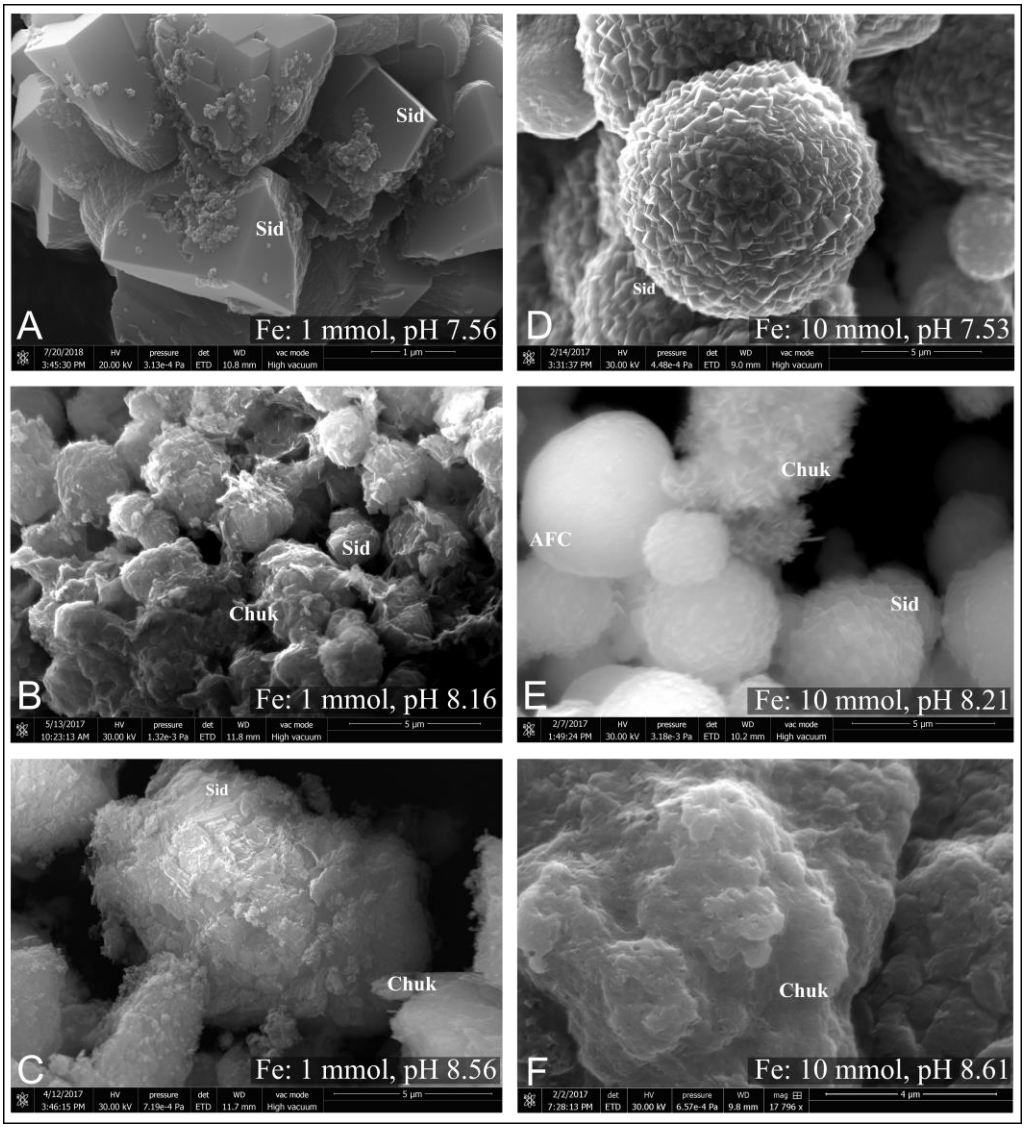

Figure 1: SEM micrographs of experimental precipitates showing representative morphological end-members. A to C) Fe concentration 1 mmol/kg, D to F) Fe concentration 10 mmol/kg. Morphological diversity is attributed to the range of siderite saturation states investigated, which in turn controls the rates of nucleation and growth. As shown from A to C and D to F, increasing pH causes precipitates to change from pure siderite to a mixture of siderite and chukanovite, to pure chukanovite. E shows a spherical particle with no apparent crystalline morphology at the resolution limit of the SEM (10s of nm), and is interpreted to be amorphous iron carbonate (AFC), which recrystallized to form the spherical clusters of rhombs, similar to polycrystalline particles shown in D.

Above pH 8, pure siderite could not be obtained. The precipitate was either a mixture of siderite and chukanovite or purely chukanovite. Between pH 8.5 and 9 the precipitates were nanocrystalline and often purely chukanovite (Fig 1c, f). Chukanovite [$Fe_2(CO_3)(OH)_2$] is an iron(II) carbonate hydroxide with acicular, platy or fibrous crystals. It is metastable with respect to siderite, and thus can transform to siderite with time (Azoulay et al., 2012). The presence of chukanovite and siderite mixed within the sample (Fig 1b, e) indicates more than one formation pathway for siderite, probably through competitive surface nucleation of the two phases on an amorphous precursor (Dideriksen et al., 2015).

The range in morphology (rhombs to spherical clusters of rhombs) is most likely influenced by the balance between nucleation and growth rates. Previous studies of Fe(II)-carbonate precursor structures and stability have shown that the amorphous precursor provides a low energy pathway to Fe(II)-carbonate mineralisation (Sel et al., 2012; Dideriksen et al., 2015). After its initial nucleation, the amorphous precursor provides a substrate for the subsequent heterogeneous nucleation of siderite (or chukanovite), as observed in other mineral systems (Van Cappellan, 1992; Nielsen et al., 2014). Rapid surface nucleation would therefore replace the initially spherical amorphous particle with a significant number of siderite rhombs encrusted on its surface (Van Cappellan, 1992; Nielsen et al., 2014). This process continues until the amorphous precursor is consumed and progressively replaced by siderite, yielding an overall morphology that Dideriksen et al. (2015)

214 argued was a distinctive product of this mineralisation pathway. This morphology is identical to that
215 observed in our experiments (Fig 1d, e). The clusters of rhombs in spherical polycrystalline
216 aggregates were primarily noted in our nucleation experiments with Fe^{2+} concentration of 10 mmol,
217 allowing a high saturation state and rapid nucleation. The rhombohedral crystal shape was
218 observed in experiments with lower Fe^{2+} concentration of 1 mmol as well as lower pH, and therefore
219 lower saturation, together promoting slower nucleation rates relative to growth rates.

220

221 ***4.2 Cation uptake in siderite***

222 **4.2.1 Mn uptake**

223 Mn uptake was observed in all experiments with Mn^{2+} present in the initial solution (a range
224 of such data from growth experiments is presented in Fig 2). Fe and Mn decreased in all growth
225 experiments with time (Fig 2). In experiment 8 at pH 8 (Fig 2), Fe and Mn show a slight increase
226 after 20 days; this pattern is observed across all cations analysed. As solution samples were
227 analysed in groups and retained in the glovebox after acidification, we interpret this to reflect
228 gradual sample evaporation in the low-humidity glovebox atmosphere with increased experiment
229 duration. During growth experiments Fe/Mn ratios increased as reactions progressed, coincident
230 with decreasing siderite saturation, which in turn led to decreasing growth rates. Because
231 experiments were conducted in closed vessels, the removal of Fe during precipitation leads to a
232 progressive decrease in siderite saturation state and therefore lower reaction rates with time. The
233 negative relationship between rate and Fe/Mn indicates (data not shown) that Mn uptake is
234 influenced by the siderite saturation state in solution.

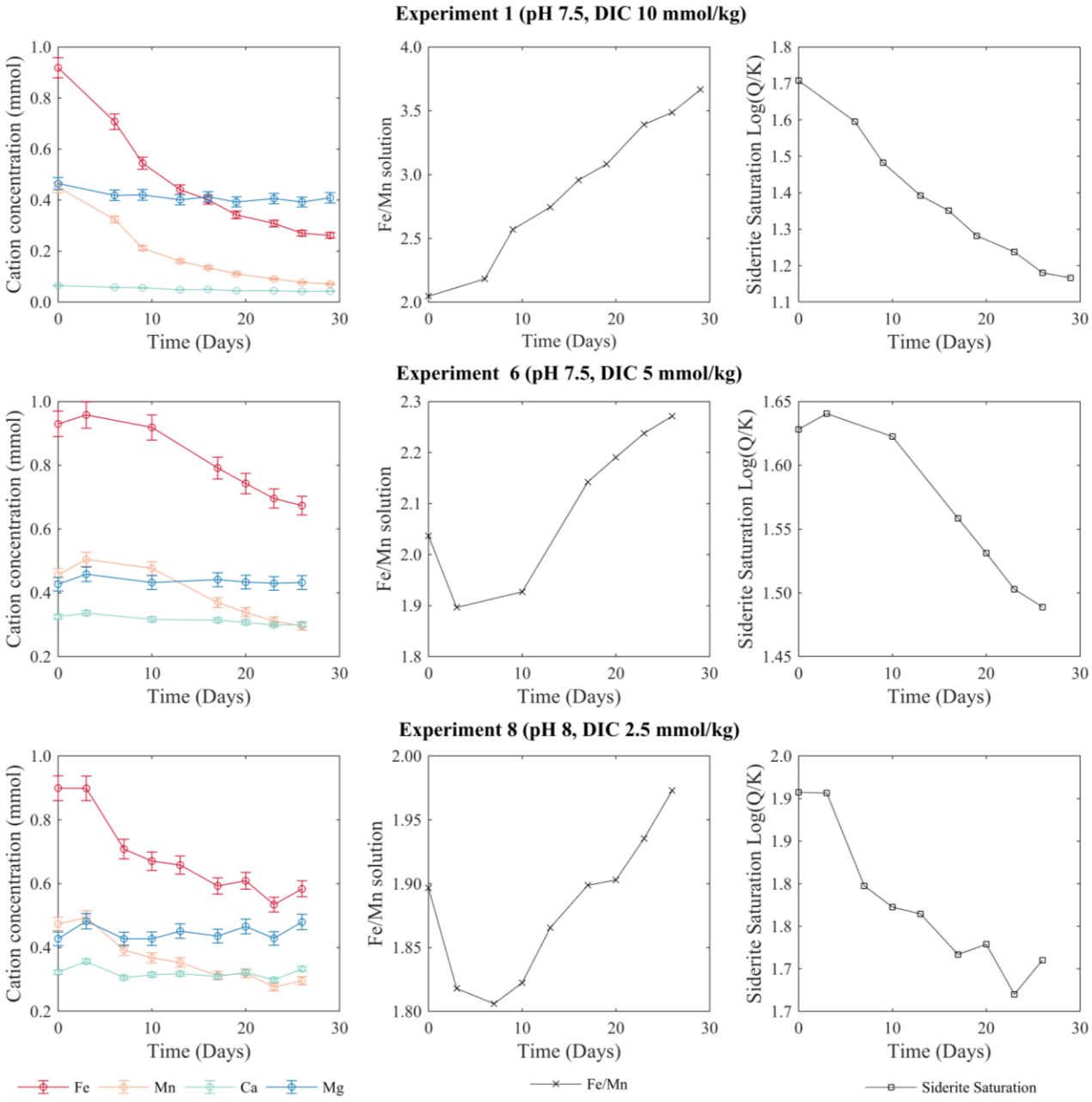

Figure 2: Selection of growth experiments displaying cation concentration in solution with time. Pure siderite seed (0.5g) was added at the start of all experiments. Fe and Mn uptake are notable. The differences in Fe uptake reflect differences in starting pH and pCO_2, and therefore saturation state, between the experiments. Fe/Mn of the solution increases with decreasing siderite saturation, indicating that Mn is incorporated into the precipitate in preference to Fe with decreasing reaction rate of siderite. Ca and Mg concentrations are generally invariable, and uptake is not discernible. The final concentrations of Ca and Mg in all experiments are within error of the initial concentration.

Fe/Mn ratios of the initial solution and the final precipitate show a strong positive correlation for both nucleation and growth experiments as shown in Fig 3, but the evolution of Fe/Mn in solution over time (Fig 2) suggests cation ratios are not the sole factor in controlling Mn uptake. The correlation between Fe/Mn of the precipitate and initial solution appears to deviate from a 1:1 line (Fig 3), although this deviation is statistically insignificant. The relationship between calculated Fe/Mn in the precipitate and the initial Fe/Mn in nucleation experiments also varies with crystalline Fe(II)-carbonate phase (siderite and chukanovite). EDS spectra and ICP-OES data from pure chukanovite samples (Fig 3) shows Mn uptake in chukanovite to be less than in siderite. However, a positive correlation is still present, regardless of the phase, as evidenced by a similar trend in the pure siderite growth experiments.

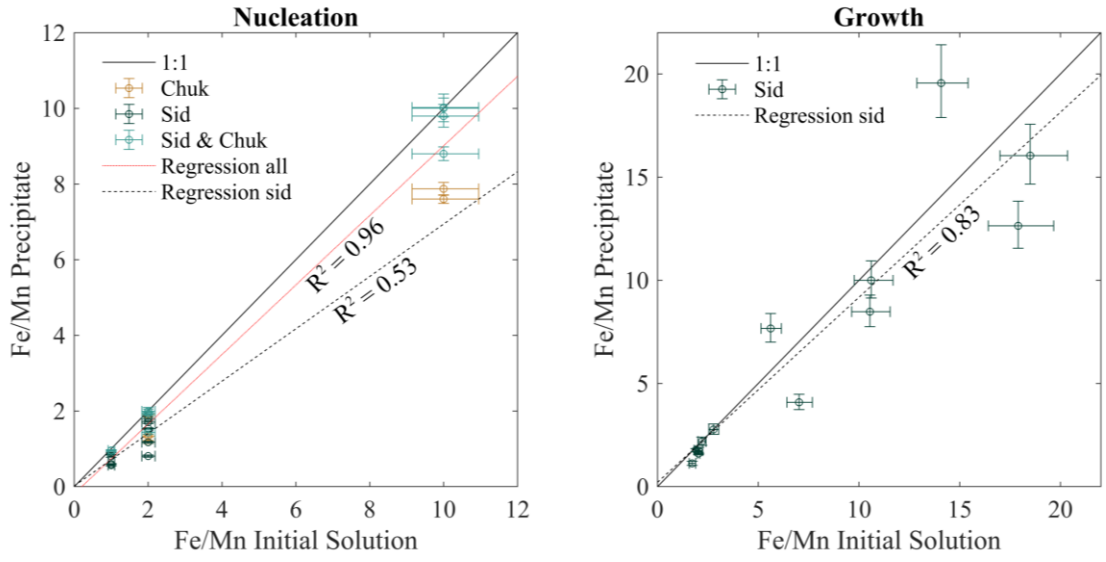

Figure 3: Fe/Mn of precipitate and initial solution in growth and nucleation experiments. Fe/Mn of final precipitate was calculated from the initial and final Fe/Mn ratios from solutions.

4.2.2 Ca uptake in siderite

For nucleation experiments, Ca was incorporated into siderite with less preference than for Mn. Ca uptake was between 10-30% of initial concentration in nucleation experiments, but correlations with factors such as pH, cation concentrations or pCO_2 were not statistically meaningful. At higher pH, Ca uptake appeared to increase, but the presence of multiple phases

complicates the interpretation of data collected from these experiments (Supplementary Information).

In contrast, during growth experiments, Ca uptake was not discernible when Mn was present (Fig 2). Although there is some variation in Ca over time, mostly noticeable in experiment 8 (Fig 2), this is likely an artefact of dilution. The final concentration of Ca is still within error of the starting concentration, and therefore Ca uptake is not discernible using ICP-OES. EDS spectra of some of the growth experiments show a very minor amount of Ca present in the precipitate (0.5- 1.6 Wt %). The amount detected also increased when the average rate of the experiment was generally higher. For instance, one experiment with an average rate of growth of 0.02 mmol/day showed 1-1.2 wt % uptake of Ca on EDS. In contrast, an experiment with a rate of a growth of 0.002 mmol/day, resulted in an EDS measurement of 0.2-0.6 wt % Ca. However, these quantities are very close to the detection limits of SEM-EDS and cannot be used for quantitative analyses. They are presented simply to support the solution chemistry data which suggests that Ca uptake was negligible during growth experiments.

Control growth experiments at low saturations were conducted with only Fe and Ca to investigate whether the presence of Mn was inhibiting Ca uptake. In these experiments there is no observable uptake of Ca under the conditions explored here, despite clear evidence for siderite growth (Fig 4). EDS spectra yielded 0.2-0.5 Wt% Ca in these control experiments.

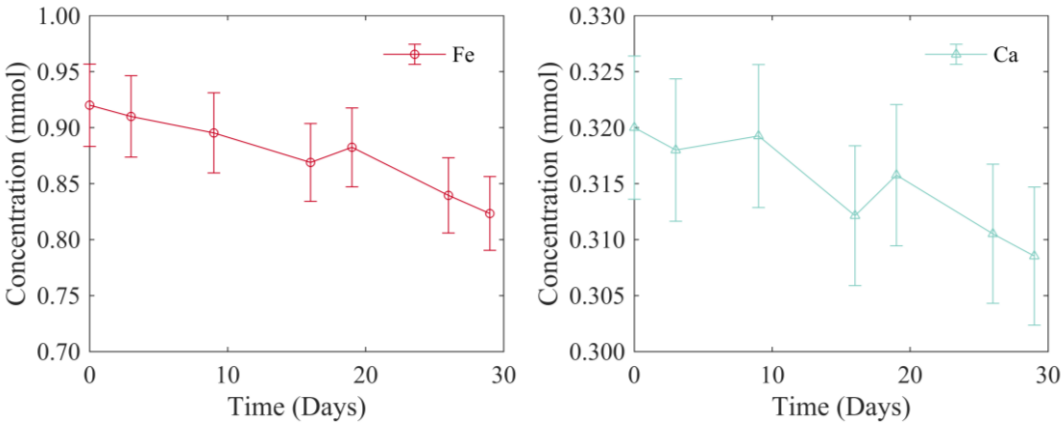

Figure 4: Control growth experiments with only Fe and Ca in starting solution showed decrease in Ca, but within error. Therefore no discernible uptake can be noted from the control experiments.

4.2.3 Mg uptake in siderite

ICP-OES data show no evidence for Mg uptake into siderite in either nucleation or growth experiments at ambient temperature. Some variation in Mg concentration is noted in Fig 2, although this is mainly in Experiment 8. Similar to the Ca concentrations discussed above, the variations in Mg can be attributed here to inconsistencies in dilution between some samples. However, the end concentration and the starting concentration of Mg are within error of each other and therefore significant Mg uptake is not detectable by ICP-OES.

As mentioned previously, nucleation experiments above pH 8 produced a mixture of siderite and chukanovite. EDS-SEM point analysis on these samples detected a small Mg peak, although it was very close to the detection limit. As this peak was noted in 60% of samples above pH 8, it could be inferred that a very minor amount of Mg may have been taken up in the chukanovite structure, but not enough to be detectable by ICP-OES. This was the case irrespective of whether Mn and/or Ca were present in solution, including at modern marine concentrations of Mg (52 mmol). Mg is known to inhibit calcite growth at seawater concentrations (Zhang and Dawe, 2000; Davis et al., 2004; Chen et al., 2005) but, in contrast, Mg did not appear to have any effect on Mn or Ca uptake in siderite in the experimental temperature and pressure ranges used, even at modern seawater concentrations.

As previous studies have considered the effect of temperature on Mg uptake in siderite (Romanek et al., 2009), two higher temperature Mg control experiments were also conducted to explore this effect further. As expected, the rate of seeded siderite growth increases with temperature (Fig 5). The 40˚C experiment yielded no evidence for Mg uptake, within analytical error. At 55˚C, Mg uptake was statistically significant, though minor, at 0.0099 mmol in total (< 2 mol % uptake). SEM-EDS point analysis detected a small Mg peak, although it is bordering on the detection limit.

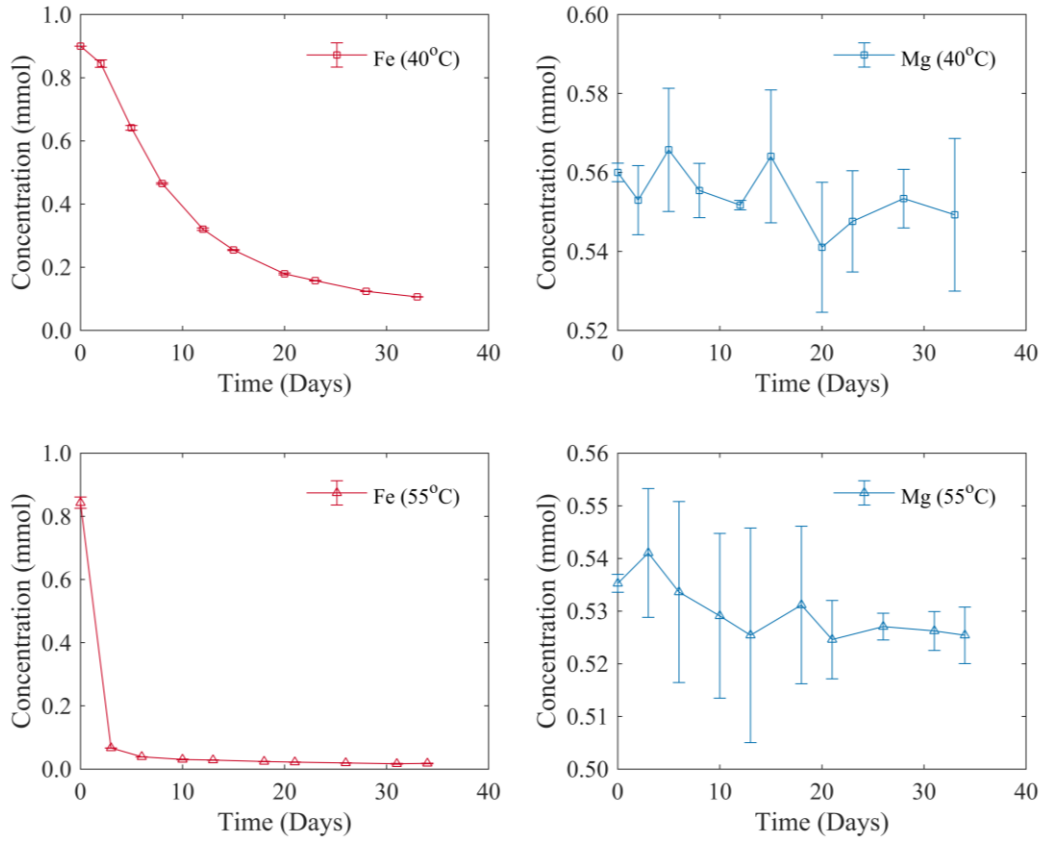

Figure 5: Control experiments with Fe and Mg as the only available cations to monitor Mg uptake in siderite at elevated temperatures, and in the absence of competing cations. Mg uptake was only discernible at 55˚C.

4.3 Rates of growth

Solution chemistry data from seeded growth experiments indicate that each experiment is associated with significant Mn uptake, in addition to Fe, into overgrowths precipitated on siderite seed material. Thus, in order to calculate growth rates as a function of solution supersaturation, we chose to evaluate supersaturation with respect to a Mn-bearing siderite with a composition equating to the average Mn coprecipitated in overgrowths (i.e., 11 mol% Mn in $FeCO_3$, or $Fe_{0.89}Mn_{0.11}CO_3$). In order to estimate the log K_{sp} for such a material, we assumed a complete binary solid solution between $MnCO_3$ and $FeCO_3$ and employed a regular solid solution model to estimate activity coefficients of solid phases (Glynn, 2000). This regular solid solution model employs the dimensionless parameter, a_0, which is used in the expansion series to estimate the excess Gibbs free energy of mixing between two end-members (Glynn, 2000). For the $(Fe,Mn)CO_3$ system, this

dimensionless parameter is constrained to a value <2.0 based on experimental data (Glynn, 2000). We used a log K_{sp} value for $FeCO_3$ equal to -10.24 (Fosbøl et al., 2010) and, for $MnCO_3$, a log K_{sp} value equal to -12.51 (Jensen et al., 2002). The resulting K_{sp} for $(Fe,Mn)CO_3$ as a function of composition is illustrated in Fig 6.

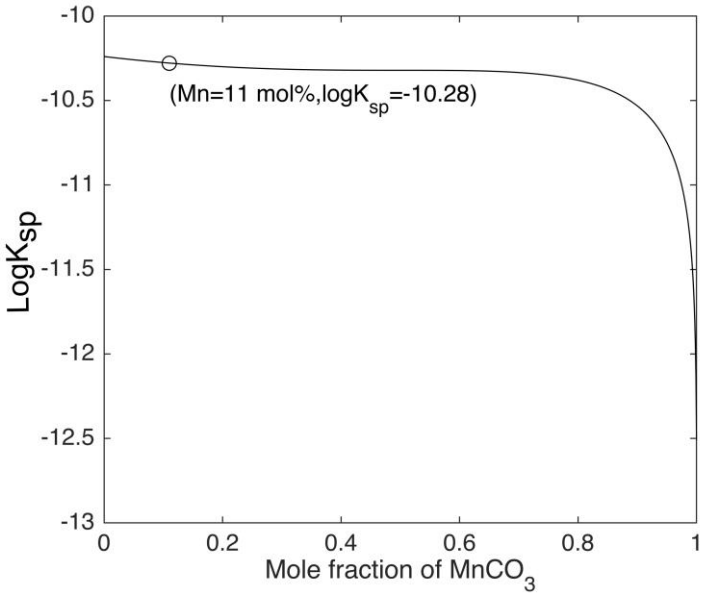

Fig 6: Calculated K_{sp} = -10.28 at Mn substitution of 11 mol% into the carbonate phase formed on average during seeded growth experiments.

Experimentally calculated surface area-normalised growth rates for seeded experiments are shown in Fig 7 as a function of supersaturation relative to $Fe_{0.89}Mn_{0.11}CO_3$. Although the data are highly scattered, a statistically significant relationship between growth rate and precipitation is evident within the 95% confidence interval. This relationship can be expressed with a general rate law for growth:

$$R = k(\Omega-1)^n$$

where R is rate (mol/m^2/hour) k is the rate constant, n is the empirical reaction order and (Ω - 1) is the supersaturation with respect to $Fe_{0.89}Mn_{0.11}CO_3$. Our data constrain n to 0.95 and k to 8.11E-8 mol/hr. The empirical reaction order is generally thought to contain information about the dominant growth mechanism (Teng et al., 2000). Kinetic studies of mineral growth typically attribute

n values of 1 to reflect adsorption-controlled growth, values of 2 to reflect growth at screw dislocations via a spiral growth mechanism, and values >2 to reflect growth at screw and edge dislocations (Teng et al., 2000). However, this general rate law does not take into account the structure and source of dislocations at the mineral surface and, because such empirical rate laws are typically derived from bulk solution chemistry measurements, do not reflect growth processes actually operating at mineral surfaces (Teng et al., 2000). From our experimental data we are unable to resolve statistically significant crossover points in the empirical reaction order as a function of supersaturation which might be taken to reflect a change in the dominant mechanism. More data will be required to elucidate this dependence, in particular direct observations of the dominant surface growth mechanism under these conditions.

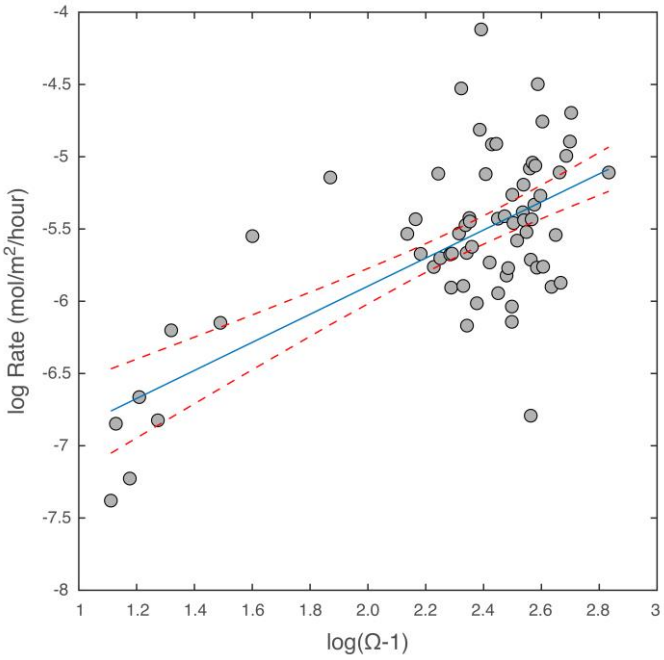

Figure 7: Experimental rates (mol//m^2/hr) from seeded growth experiments. Dashed lines indicate 95% confidence intervals.

4.4 Effect of salinity changes

As mentioned in Table 1, salinity changes were explored using NaCl concentrations analogous to fresh, brackish and marine waters, in the presence of Fe, Mg, Ca and Mn as available cations.

However, salinity changes were found to have no significant effect on the uptake behaviours described in the above sections (Supplementary Information).

5 Discussion

5.1 Comparison to previous studies

5.1.1 Trace element uptake in siderite

In their examination of the partitioning of trace elements between carbonate minerals and aqueous solutions, Rimstidt et al. (1998) observed that, for calcite, the apparent distribution coefficients derived from experimental work correlated with the quotient of the solubility product of the host carbonate to the trace element carbonate. The authors also extended this analysis to siderite, using an experimental dataset reported previously (Thornber and Nickel, 1976). To facilitate comparison to our experimental data, we have also estimated apparent trace element distribution coefficients for siderite from Romanek et al. (2009), plotted in Fig 8.

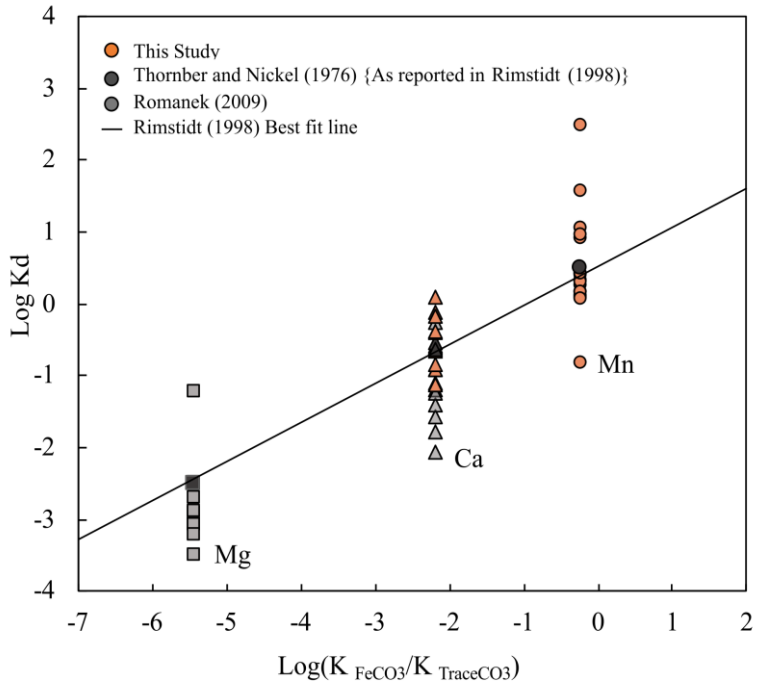

Figure 8: Comparisons of apparent distribution coefficients (Kd') from Romanek et al (2009), Rimstidt et al (1998) and calculated Log K (Rimstidt et al., 1998)*. Kd is positively correlated to the*

solubility quotient of siderite with respect to trace cation, displaying a clear preference of Mn uptake over Ca and Mg.

Our data support the initial observation by Rimstidt et al. (1998) that, in addition to calcite, trace element incorporation into siderite correlates with the quotient of the siderite and trace element carbonate solubility products. Although available experimental data show significant variation about this trend, this general correlation leads to two conclusions. The first is that, as our experiments show, trace element uptake into siderite should occur with increasing preference in the following order: Mg << Ca < Mn; this finding is consistent with Rimstidt et al (1998). Romanek et al. (2009) have previously shown a linear relation between Ca:Fe(aq) and Ca:Fe(s) in the absence of Mn but presence of Mg. This, along with the low Kd of Ca compared to Mn, also implies that Ca uptake is hindered by the presence of the preferential trace cation Mn.

The second conclusion, noted by Rimstidt et al. (1998), is that the slope of the correlation deviates from the equilibrium slope of 1, meaning that kinetic processes rather than equilibrium processes ultimately control trace element incorporation into siderite during nucleation and/or growth.

In the discussion that follows, we provide a review of the factors behind these apparent trends in element uptake during siderite growth, and discuss these factors with respect to reported compositional data for ancient siderites.

5.2 Mechanisms of cation uptake in siderite

5.2.1 Cation hydration characteristics

Free ions (such as Fe^{2+}, Mn^{2+} etc.) in aqueous solution are closely associated with H_2O molecules. Dehydration energies required for a cation to be extracted from these hydrating H_2O molecules, and become incorporated to a growing crystal surface, are dependent on cation size and charge. Romanek et al. (2009) attributed the lack of Mg uptake during siderite growth at ambient temperature to a higher dehydration energy required for Mg^{2+} as opposed to Ca^{2+} and Fe^{2+}. However, the hydration enthalpies of Mg^{2+} and Fe^{2+} are, in fact, very similar (Burgess, 1978). Our

data show that observable Mg uptake does not occur during nucleation or growth at ambient temperatures, regardless of solution chemistry. The presence of Mg also does not appear to affect the uptake of other cations, where the main trend was a preference for proportional Mn uptake. Finally, if dehydration was a main kinetic control, the relative hydration energies would predict preferential uptake of Ca over Mn, the opposite to what is observed in our data and in previous studies (Fig 8). Together, this indicates that other factors must be primarily responsible for cation uptake during siderite growth.

5.2.2 Crystal structure

The preference for Mn^{2+} uptake over Ca^{2+} and Mg^{2+} during siderite growth could relate partly to structural differences between rhombohedral carbonates. Intuitively, we might expect cations with a similar radius to iron to be accommodated more readily in the siderite structure. Reeder (1983), based on experimental work summarised by Goldsmith (1983), suggested that the differences in ionic radius between cation pairs in rhombohedral carbonates could be divided into two classes: pairs that should exhibit complete miscibility (differences ≤ 0.11Å), and those that should exhibit limited miscibility (differences ≥ 0.11Å). On this basis, cation radius differences between Fe^{2+} and Mn^{2+} and Fe^{2+} and Mg^{2+} predict complete miscibility, whereas Fe^{2+} and Ca^{2+} predict limited miscibility. To a first approximation, this suggests that there may be few structural barriers to extensive Mn incorporation in the siderite lattice, consistent with our Mn uptake data. In addition, these relationships suggest that structural factors may limit the amount of Ca incorporation in the siderite lattice, which may be one factor contributing to the observed low distribution coefficients for Ca. The prediction of full miscibility between Mg and Fe in siderite, however, suggests that the negligible uptake observed in our experiments and low apparent distribution coefficients (Thornber and Nickel, 1976; Rimstidt et al., 1998; Romanek et al., 2009) may be better explained by kinetic factors.

5.2.3 Surface structural control

Mineral growth mechanisms are strongly controlled by saturation state, implying that the structure of the siderite surface, as it grows in solution, may control trace element uptake. In general, with increasing supersaturation, mineral growth progresses from spiral growth triggered at surface kink sites, to 2D nucleation, and non-classical growth (possibly involving an amorphous precursor) above what is termed the roughening transition (Sunagawa, 2007; Rodriguez-Navarro et al., 2016). However, most natural systems are poised at saturation states that promote spiral growth, which features the advancement of structurally non-equivalent growth steps on growth hillocks (Paquette and Reeder, 1995; Rakovan and Reeder, 1996; Reeder and Rakovan, 1999; Sunagawa, 2007). Previous work on calcite has shown that during spiral growth, trace element uptake is strongly controlled by both the rates of growth step advancement and by structural characteristics of kink sites generated at non-equivalent growth faces (Paquette and Reeder, 1995; Reeder, 1996; Rakovan and Reeder, 1996). This process ultimately results in intra-sectoral zoning of trace elements on the calcite surface (Paquette and Reeder, 1990). This work also suggests that cation size may play a role in determining trace element incorporation at the growing interface, with sterically unconstrained kink sites favouring larger cations and more constricted kink sites favouring smaller cations (Paquette and Reeder, 1995; Rakovan and Reeder, 1996). This work offers a conceptual framework to explain differential element incorporation and variations with growth rate, as we have documented for Mn incorporation. Specifically, increases in growth rate will translate to increases in the rate of growth step advancement (Gratz et al., 1993). However, different growth steps exposed on symmetrically non-equivalent faces will respond differently to saturation state. On this basis, one explanation for our observed decrease in Mn uptake with increases in growth rates may be that growth rate increases translate to more rapid advancement of growth steps at the siderite surface where Mn incorporation is less favoured, perhaps by surface structural constraints.

Another possibility is that if growth rates of siderite increase to the point where a different growth mechanism begins to dominate (i.e., 2D nucleation), then trace element incorporation may exhibit corresponding differences. However, although the saturation state at which 2D nucleation

might begin to dominate siderite growth is unconstrained, our growth rate data cannot statistically resolve changes in the empirical reaction order, or the relationship between growth rate and saturation state which might signal a mechanism change.

5.2.4 Transport / boundary layer control

An additional kinetic control, discussed by Rimstidt et al. (1998), involves the transport of trace elements through solution to the surface of the growing crystal. Because trace elements are likely to be incorporated at rates that differ from the rate of Fe^{2+} incorporation into siderite, this may lead to the development of a solution boundary layer that is either depleted in the trace element (i.e., if Kd > 1) or enriched in the trace element (i.e., if Kd < 1). This will, in turn, influence the effective Kd, rate of cation diffusion to the growing surface, and/or influence the overall growth rate of the mineral (i.e., lead to oscillatory zoning; Reeder et al., 1990; Wang and Merino, 1992).This relationship predicts that trace elements where the apparent distribution coefficient is >1 should exhibit an increase in element uptake with decreasing growth rate. Indeed, our observations of Mn uptake suggest that this process may be operating, analogous to Mn uptake in calcite (Dromgoole and Walter, 1990). However, as discussed above, because surface structural controls on element uptake may also be important in our system, we cannot uniquely identify which processes are most important. Indeed, both may be operating, leading to a network of complex kinetic controls on element uptake.

The boundary layer is likely to shrink with increasing temperature due to increased rates of diffusion. This would minimise the role of the diffusion layer in controlling cation uptake. However, despite these expectations, available data indicate a number of competing factors as temperature increases. For example, Rimstidt et al. (1998) showed that modelled Kd values for numerous cations in calcite do not change significantly over 0-100˚C and attributed this to solubility products of carbonates changing similarly with temperature. In their model, however, the Kd of Mg in calcite increased with temperature. We return to the influence of temperature on Mg uptake in siderite in section 5.2.6.

5.2.5 Non Traditional Precipitation Pathways

As discussed above, there seem to be few structural constraints limiting the extent of Mg incorporation into the siderite structure, yet Mg uptake in siderite is characterised by very low distribution coefficients. This is analogous to the incorporation of Mg in calcite, which is characterised by similarly low distribution coefficients (Reeder, 1983; Rimstidt et al., 1998; Romanek et al, 2009). Yet, Mg-rich calcite is well known from modern and some ancient marine carbonate successions, and notably from biologically-mediated calcite precipitation (Weiss et al., 2002; Addadi et al., 2003; Politi et al., 2009). Recent studies of carbonate precipitation kinetics have shown that the formation of an amorphous calcium carbonate (ACC) precursor permits significant Mg-incorporation upon precipitation (Blue and Dove, 2015). The Mg content of the ACC depends strongly on pH and Mg concentration in solution. As ACC recrystallises, the resulting calcite is often characterised by relatively high Mg content (Blue et al., 2017). The precipitation of ACC itself requires very high supersaturation states in the $CaCO_3$ system (Brečević and Nielsen, 1989) which, as previous studies have shown, can be attained in biomineralizing systems through the specific roles of biomolecules (Weiner and Dove, 2003). Amorphous precursor phases also feature commonly in the Fe(II)-carbonate system, in particular during homogeneous nucleation (Dideriksen *et al.*, 2015; Jiang and Tosca*.,* 2019). Such a pathway might be common in systems that achieve rapid supersaturation with respect to siderite. One example is through dissimilatory Fe-reduction where Fe^{2+}, DIC, and total alkalinity are all simultaneously increased as the reaction progresses. In fact, experimental studies of dissimilatory Fe-reduction show morphological evidence for precipitation of siderite through an amorphous iron carbonate (AFC) precursor (Mortimer et al., 1997; Johnson et al., 2005; Dideriksen et al., 2015).

Such precipitation pathways in the Fe(II)-carbonate system might be expected to influence element incorporation in to the siderite structure, given that amorphous $CaCO_3$ has been shown to

499 be relatively indiscriminate toward trace element uptake (Littlewood et al., 2017). Our homogeneous
500 nucleation experiments producing siderite via an amorphous precursor phase, however, show no
501 discernible increase in Mg. EDS-SEM detects only a small peak for Mg, barely above detection limit.
502 This is in agreement with other studies showing low apparent Kd of Mg in siderite (Thornber and
503 Nickel, 1976; Romanek et al., 2009). There is, however, one notable exception. Romanek et al
504 (2009) reported that Mg was only incorporated in to siderite structure when Mg starting
505 concentration was at modern seawater concentrations along with increased temperature and/or
506 very large increases in carbonate alkalinity. However, it is unclear from their data whether Mg
507 uptake is uniquely confined to siderite or instead to a Mg-rich carbonate phase, as the precipitates
508 reported include multiple carbonate phases (i.e., siderite and magnesite or hydromagnesite).

509 **5.2.6 The role of temperature**

510 A number of studies have documented strong increases in the distribution coefficient
511 describing Mg incorporation into calcite with temperature (Katz, 1973; Oomori et al., 1987; Mucci,
512 1987) Data for Mg^{2+} incorporation into siderite with temperature are far more limited. Data reported
513 by Romanek et al. (2009) show uptake of Mg at 70˚C, consistent with analogous predictions from
514 the $CaCO_3$ system (Romanek et al., 2009). However, the precipitate identified was magnesite or
515 hydromagnesite, where Fe becomes a trace cation. Our 40˚C experiment did not show Mg uptake
516 above the margin of error, however the precipitate formed at 55˚C did co-precipitate Mg (consuming
517 <2% of the initial concentration of Mg). Mg concentrations used in our experiments were 40-50%
518 lower than Fe concentrations, and siderite was verified through XRD. Our limited data predict that
519 Mg uptake into siderite may continue to increase with increasing temperature. Therefore, in the
520 absence of other clear controls on Mg incorporation into siderite, we consider temperature as one of
521 the strongest controls on Mg concentrations in light of available data.

522 ***5.3 Elemental composition of siderite as an indicator for paleo-environment***

523 One of the motivating scientific questions for this study is whether major element
524 composition of siderite can be a reliable paleo-environmental indicator of pore water conditions,

525 applicable to continental siderite studies through the Phanerozoic. Elemental compositions of
526 sphaerosiderites and other early diagenetic forms of siderite have been reported in many studies
527 (Mozley, 1989; Baker et al., 1996; Choi et al., 2003; Lim et al., 2004; Ufnar et al., 2004a; Robinson
528 et al., 2010; Ludvigson et al., 2013; Passey, 2014; Weibel et al., 2016). Some of these studies
529 report similar compositional trends, notably the repeated observation of Mn rich cores and Ca and
530 Mg rich outer rims/overgrowths (Curtis et al., 1986; Baker et al., 1996; Choi et al., 2003; Lim et al.,
531 2004; Passey, 2014; Weibel et al., 2016). Other examples show only minor Ca, Mg and Mn
532 substitution, with Mn incorporated the least (Choi et al., 2003; Robinson et al., 2010). Generally,
533 extensive Ca or Mg substitution, or extensive substitutions of cations other than Fe^{2+} have been
534 considered to indicate marine alteration (Mozley, 1989; Choi et al., 2003; Lim et al., 2004; Ufnar et
535 al., 2004a; Robinson et al., 2010; Weibel et al., 2016).

536 Our results indicate that the cation chemistry in solution alone has little bearing on elemental
537 uptake in siderite. Instead, each trace cation (Mn, Ca, Mg) has a distinctly different uptake
538 behaviour, affected by concentration, siderite saturation, presence of other competing cations,
539 crystal structural controls, and growth mechanisms. For example, our results indicate that Mn
540 uptake from natural pore waters would be preferential even if Ca and Mg concentrations are high
541 (i.e., marine). Our results also indicate Fe/Mn ratios of the solution to be reflected in the Fe/Mn
542 ratios of the precipitate, and so high Mn substitution in geological siderite could simply indicate a
543 relatively high Mn content in the pore waters, and not impure siderites reflecting a marine influence
544 as suggested in Choi and Kim (2006). Further to this, our results imply that observations of “Ca-rich
545 siderite” are problematic and suffer from a lack of supporting evidence from the crystal growth
546 literature. The most parsimonious explanation is that other factors must be at play in a natural
547 system allowing Ca uptake into siderite. Comparison of experimental and geological examples of
548 siderite also sheds light on the origins of Mg enrichment in geological siderites. Given current
549 constraints on Mg incorporation and partition coefficients, rather than marine influences, Mg-
550 enriched overgrowths on rims of sphaerosiderites could perhaps be explained as products of

551 diagenesis at shallow burial temperatures (Curtis et al., 1986; Mozley and Wersin, 1992; Baker et
552 al., 1996; Choi et al., 2003; Lim et al., 2004; Passey, 2014; Weibel et al., 2016).

553 Another origin of Mg-enriched compositions may be the presence of additional carbonate
554 minerals. For instance, if Ca-Mg carbonate was present in the initial mineral assemblage, its
555 recrystallisation to siderite is thermodynamically favoured if pore water Fe^{2+} concentrations are 5%
556 of Ca^{2+} concentrations (Berner, 1971). Evidence of the growth of Ca-Mg carbonate and siderite in
557 the same environment, including in the same concretion, can be found in wetland intertidal marsh
558 sediments in Norfolk, UK, reported by Pye et al. (1990). The siderite cements from these
559 concretions do not show Mg enrichment, instead Mg is enriched in the calcite cement growing in the
560 same concretion. As most studies determine elemental compositions using electron microprobe,
561 carbonate phases are typically not identified unambiguously (for instance, through XRD). Therefore,
562 the reported Ca-Mg-Mn substitutions could alternatively be interpreted as physical mixtures of
563 zoned carbonates, such as those examined by Pye et al. (1990).

564 Finally, one puzzling feature of geological siderite relates to the low, but non-negligible,
565 background concentrations of Mg in almost all natural siderites (0.5 - 2 Wt %) (Choi et al., 2003;
566 Ufnar et al., 2004a; Robinson et al., 2010; Weibel et al., 2016). The two mechanisms of Mg
567 enrichment (temperature increases or Ca-Mg carbonate replacement) suggested here do not readily
568 apply to all examples where this has been observed. One remaining consideration could be the role
569 of organic macromolecules during siderite precipitation. For instance, in calcium carbonate, it has
570 been shown that carboxylated proteins, and other biomolecules, influence the uptake of Mg
571 (Stephenson et al., 2008; Wang et al., 2009). In one study, carboxylated proteins with more of an
572 affinity for binding Ca allowed production of Mg-rich amorphous calcium carbonate similar to high-
573 Mg calcite or dolomite. The ratios of Mg/Ca depended on the binding properties of the organic
574 molecules involved (Wang et al., 2009). In a wetland system, rich in organic by-products, biological
575 macromolecules could be similarly influencing the growth of siderite, allowing deviation in cation
576 uptake behaviour from those observed in classical abiotic crystal growth. Assessing this is beyond
577 the scope of this study and merits further work, and whether or not the background Mg values noted

in siderite could perhaps be a signal of biological activity must await further experimental and observational evidence. Nonetheless, our study provides key abiotic constraints in elemental uptake for siderite growth in saturations more analogous to natural waters than previous studies, which can be used to better our understanding of the offsets between abiotic and biotic pathways.

The elemental composition of siderite clearly reflects a variety of growth conditions, and thus cannot be solely used to infer palaeoenvironment. Instead, we suggest siderites should be studied in the wider context of the sedimentology and stratigraphy of the units they grew within, with detailed petrography and mineralogy of the spheres, as well as isotopic and elemental composition, to have a broad understanding of their growth conditions, and assess their suitability for palaeoclimate reconstruction.

6 Conclusions

Our experimental results provide new insight into the coprecipitation of Mn, Ca, and Mg during siderite nucleation and growth. This expanding experimental dataset emphasises the role of kinetic factors in regulating trace element incorporation into siderite, in particular surface structural controls during growth, transport phenomena, and temperature. In reality, because multiple factors regulate trace element incorporation, general and quantitative relationships between mineral chemistry and solution composition are difficult to ascertain and thus palaeoenvironmental interpretations should be made with these factors in mind.

Nevertheless, although experimental results provide valuable mechanistic information on the chemical controls on siderite composition, discrepancies between synthetic and natural systems still persist. Available data indicate that the apparent differences in the Mg and/or Ca concentration of both natural and synthetic siderite may in fact arise from incomplete mineralogical and geochemical characterisation. In order to address this issue more quantitatively, new and robust datasets, including complete characterisation of all crystalline carbonate phases within natural and synthetic samples, will be required. This should further illuminate the relationship between mineral chemistry

603 and depositional environment and the potential for natural siderite specimens to reveal paleoclimatic
604 information through their chemical and/or isotopic composition.

605 7 Acknowledgements

606 This study was funded by NERC as part of the Doctoral Training Partnership in Environmental
607 Research at the University of Oxford (NE/L002612/1). The authors would like to thank Rosalie
608 Tostevin and Clancy Jiang for help with experimental setup, analyses and interesting discussions,
609 and the three anonymous reviewers for thoughtful comments. The authors also thank Kat Clayton
610 and Alice Barroll for assistance with XRD analyses, Gillian Mackinnon and John McArthur for help
611 with ICP-OES analyses, and Jon Wade and Phil Gopon for assistance with SEM imaging.

612

613 8 References

614 Addadi L., Raz S. and Weiner S. (2003) Taking advantage of disorder: Amorphous calcium
615 carbonate and its roles in biomineralization. *Adv. Mater.* **15**, 959–970.

616 Azoulay I., Rémazeilles C. and Refait P. (2012) Determination of standard Gibbs free energy of
617 formation of chukanovite and Pourbaix diagrams of iron in carbonated media. *Corros. Sci.* **58**,
618 229–236. Available at: https://www.sciencedirect.com/science/article/pii/S0010938X12000674.

619 Bahrig B. (1989) Stable isotope composition of siderite as an indicator of the paleoenvironmental
620 history of oil shale lakes. *Palaeogeogr. Palaeoclimatol. Palaeoecol.* **70**, 139–151.

621 Baker J. C., Kassan J. and Hamilton P. J. (1996) Early diagenetic siderite as an indicator of
622 depositional environment in the Triassic Rewan Group, southern Bowen Basin, eastern
623 Australia. *Sedimentology* **43**, 77–88. Available at: 10.1016/0031-0182(89)90085-0.

624 Berner R. A. (1971) *Principles of Chemical Sedimentology*., McGraw Hill.

625 Blue C. R. and Dove P. M. (2015) Chemical controls on the magnesium content of amorphous

626 calcium carbonate. *Geochim. Cosmochim. Acta* **148**, 23–33. Available at:
627 https://www.sciencedirect.com/science/article/pii/S0016703714004980

628 Blue C. R., Giuffre A., Mergelsberg S., Han N., De Yoreo J. J. and Dove P. M. (2017) Chemical and
629 physical controls on the transformation of amorphous calcium carbonate into crystalline
630 CaCO3 polymorphs. *Geochim. Cosmochim. Acta* **196**, 179–196. Available at:
631 https://www.sciencedirect.com/science/article/pii/S0016703716305178

632 Brečević L. and Nielsen A. E. (1989) Solubility of amorphous calcium carbonate. *J. Cryst. Growth*
633 **98**, 504–510. Available at:
634 https://www.sciencedirect.com/science/article/pii/0022024889901681

635 Burgess J. (1978) *Metal ions in solution*., Ellis Horwood Limited, Chichester.

636 Butler I. B., Schoonen M. A. A. and Rickard D. T. (1994) Removal of dissolved oxygen from water: A
637 comparison of four common techniques. *Talanta* **41**, 211–215. Available at:
638 https://www.sciencedirect.com/science/article/pii/003991409480110X

639 Van Cappellan P. (1992) The formation of marine apatite: A kinetic study. Yale University.

640 Carothers W. W., Adami L. H. and Rosenbauer R. J. (1988) Experimental oxygen isotope
641 fractionation between side&-water and phosphoric acid liberated CO+iderite. *Geochem n*
642 *Cosmochim. Ada* **52**, 2445–2450.

643 Chen T., Neville A. and Yuan M. (2005) Assessing the effect of Mg2+ on CaCO3 scale formation–
644 bulk precipitation and surface deposition. *J. Cryst. Growth* **275**, e1341–e1347. Available at:
645 http://www.sciencedirect.com/science/article/pii/S0022024804016616.

646 Choi K. and Kim S. P. (2006) Late Quaternary evolution of macrotidal Kimpo tidal flat, Kyonggi Bay,
647 west coast of Korea. *Mar. Geol.* **232**, 17–34.

Choi K. S., Khim B. K. and Woo K. S. (2003) Spherulitic siderites in the Holocene coastal deposits of Korea (eastern Yellow Sea): Elemental and isotopic composition and depositional environment. *Mar. Geol.* **202**, 17–31.

Curtis C. D., Coleman M. L. and Love L. G. (1986) Pore water evolution during sediment burial from isotopic and mineral chemistry of calcite, dolomite and siderite concretions. *Geochim. Cosmochim. Acta* **50**, 2321–2334.

Davis K. J., Dove P. M., Wasylenki L. E. and De Yoreo J. J. (2004) Morphological consequences of differential Mg2+ incorporation at structurally distinct steps on calcite. *Am. Mineral.* **89**, 714–720. Available at: http://dx.doi.org/10.2138/am-2004-5-605.

Dideriksen K., Frandsen C., Bovet N., Wallace A. F., Sel O., Arbour T., Navrotsky A., De Yoreo J. J. and Banfield J. F. (2015) Formation and transformation of a short range ordered iron carbonate precursor. *Geochim. Cosmochim. Acta* **164**, 53–70. Available at: http://dx.doi.org/10.1016/j.gca.2015.05.005.

Driese S. G., Ludvigson G. A., Roberts J. A., Fowle D. A., González L. A., Smith J. J., Vulava V. M. and McKay L. D. (2010) Micromorphology and stable-isotope geochemistry of historical pedogenic siderite formed in PAH-contaminated alluvial clay soils, Tennessee, USA. *J. Sediment. Res.* **80**, 943–954.

Dromgoole E. L. and Walter L. M. (1990) Iron and manganese incorporation into calcite: Effects of growth kinetics, temperature and solution chemistry. *Chem. Geol.* **81**, 311–336. Available at: https://www.sciencedirect.com/science/article/pii/000925419090053A

Fisher Q. J., Raiswell R. and Marshall J. D. (1998) Siderite concretions from nonmarine shales (Westphalian A) of the Pennines, England; controls on their growth and composition. *J. Sediment. Res.* **68**, 1034–1045. Available at: https://pubs.geoscienceworld.org/jsedres/article/68/5/1034-1045/98939

672 Fosbøl P. L., Thomsen K. and Stenby E. H. (2010) Review and recommended thermodynamic
673 properties of FeCO 3. *Corros. Eng. Sci. Technol.* **45**, 115–135. Available at:
674 http://www.tandfonline.com/doi/full/10.1179/174327808X286437

675 Glynn P. (2000) Solid-Solution Solubilities and Thermodynamics: Sulfates, Carbonates and Halides.
676 *Rev. Mineral. Geochemistry* **40**, 481–511. Available at: https://doi.org/10.2138/rmg.2000.40.10.

677 Goldschmidt J. R. (1983) Phase relations of rhombohedral carbonates. *Rev. Mineral. Geochemistry*
678 **11**, 49-76.

679 Gratz A. J., Hillner P. E. and Hansma P. K. (1993) Step dynamics and spiral growth on calcite.
680 *Geochim. Cosmochim. Acta* **57**, 491–495. Available at:
681 https://www.sciencedirect.com/science/article/pii/0016703793904497

682 Jensen D. L., Boddum J. K., Tjell J. C. and Christensen T. H. (2002) The solubility of rhodochrosite (
683 MnCO 3) and siderite (FeCO 3) in anaerobic aquatic environments. **17**, 503–511.

684 Jiang C. Z. and Tosca N. J. (2019) Fe(II)-carbonate precipitation kinetics and the chemistry of
685 anoxic ferruginous seawater. *Earth Planet. Sci. Lett.* **506**, 231–242.

686 Jimenez-Lopez C. and Romanek C. S. (2004) Precipitation kinetics and carbon isotope partitioning
687 of inorganic siderite at 25oC and 1 atm. *Geochim. Cosmochim. Acta* **68**, 557–571.

688 Johnson C. M., Beard B. L., Klein C., Beukes N. J. and Roden E. E. (2008) Iron isotopes constrain
689 biologic and abiologic processes in banded iron formation genesis. *Geochim. Cosmochim.*
690 *Acta* **72**, 151–169.

691 Johnson C. M., Roden E. E., Welch S. A. and Beard B. L. (2005) Experimental constraints on Fe
692 isotope fractionation during magnetite and Fe carbonate formation coupled to dissimilatory
693 hydrous ferric oxide reduction. *Geochim. Cosmochim. Acta* **69**, 963–993. Available at:
694 https://www.sciencedirect.com/science/article/pii/S0016703704005678

695 Kandegedara A. and Rorabacher D. B. (1999) Noncomplexing tertiary amines as “better” buffers
696 covering the range of pH 3-11. Temperature dependence of their acid dissociation constants.
697 *Anal. Chem.* **71**, 3140–3144.

698 Katz A. (1973) The interaction of magnesium with calcite during crystal growth at 25–90°C and one
699 atmosphere. *Geochim. Cosmochim. Acta* **37**, 1563–1586. Available at:
700 https://www.sciencedirect.com/science/article/pii/0016703773900914

701 Khim B.-K., Choi K.-S., Park Y.-A. and Oh J.-K. (1999) Occurrence of authigenic siderites in the
702 Early Holocene coastal deposit in the west coast of Korea: an indicator of depositional
703 environment. *Geosci. J.* **3**, 163–170. Available at: http://link.springer.com/10.1007/BF02910272

704 Khim B.-K., Choi K.-S. and Park Y. A. (2000) Elemental composition of siderite grains in early-
705 Holocene deposits of Youngjong Island (west coast of Korea), and its palaeoenvironmental
706 implications. *Proc. Mar. Sci.* **2**, 205–217. Available at:
707 https://www.sciencedirect.com/science/article/pii/S1568269200800170

708 Lim D. I., Jung H. S., Yang S. Y. and Yoo H. S. (2004) Sequential growth of early diagenetic
709 freshwater siderites in the Holocene coastal deposits, Korea. *Sediment. Geol.* **169**, 107–120.

710 Littlewood J. L., Shaw S., Peacock C. L., Bots P., Trivedi D. and Burke I. T. (2017) Mechanism of
711 Enhanced Strontium Uptake into Calcite via an Amorphous Calcium Carbonate Crystallization
712 Pathway. *Cryst. Growth Des.* **17**, 1214–1223. Available at:
713 http://pubs.acs.org/doi/10.1021/acs.cgd.6b01599

714 Ludvigson G. A., González L. A., Fowle D. A., Roberts J. A., Driese S. G., Villarreal M. A., Smith J.
715 J. and Suarez M. B. (2013) Paleoclimatic Applications and Modern Process Studies of
716 Pedogenic Siderite. *New Front. Paleopedol. Terr. Paleoclimatology*, 79–87.

717 Ludvigson G. A., González L. A., Metzger R. A., Witzke B. J., Brenner R. L., Murillo A. P. and White

718 T. S. (1998) Meteoric sphaerosiderite lines and their use for paleohydrology and
719 paleoclimatology. *Geology* **26**, 1039–1042.

720 Mortimer R. J. G., Coleman M. L. and Rae J. E. (1997) Effect of bacteria on the elemental
721 composition of early diagenetic siderite: Implications for palaeoenvironmental interpretations.
722 *Sedimentology* **44**, 759–765.

723 Mozley P. S. (1989) Relation between depositional environment and the elemental composition of
724 early diagenetic siderite. *Geology* **17**, 704–706.

725 Mozley P. S. and Wersin P. (1992) Isotopie composition of siderite as an indicator of depositional
726 environment. *Geology* **20**, 817–820.

727 Mucci A. (1987) Influence of temperature on the composition of magnesian calcite overgrowths
728 precipitated from seawater. *Geochim. Cosmochim. Acta* **51**, 1977–1984. Available at:
729 https://www.sciencedirect.com/science/article/pii/0016703787901864

730 Nielsen M. H., Aloni S. and De Yoreo J. J. (2014) In situ TEM imaging of CaCO3 nucleation reveals
731 coexistence of direct and indirect pathways. *Science (80-.).* **345**, 1158 LP – 1162. Available at:
732 http://science.sciencemag.org/content/345/6201/1158.abstract.

733 Oomori T., Kaneshima H., Maezato Y. and Kitano Y. (1987) Distribution coefficient of Mg2+ ions
734 between calcite and solution at 10–50°C. *Mar. Chem.* **20**, 327–336. Available at:
735 https://www.sciencedirect.com/science/article/pii/0304420387900661

736 Paquette J. and Reeder R. J. (1990) New type of compositional zoning in calcite: Insights into
737 crystal-growth mechanisms. *Geology* **18**, 1244–1247. Available at:
738 https://pubs.geoscienceworld.org/geology/article/18/12/1244-1247/198549

739 Paquette J. and Reeder R. J. (1995) Relationship between surface structure, growth mechanism,
740 and trace element incorporation in calcite. *Geochim. Cosmochim. Acta* **59**, 735–749. Available

741 at: https://www.sciencedirect.com/science/article/pii/001670379500004J

742 Passey S. R. (2014) The habit and origin of siderite spherules in the Eocene coal-bearing Prestfjall
743 Formation, Faroe Islands. *Int. J. Coal Geol.* **122**, 76–90. Available at:
744 https://www.sciencedirect.com/science/article/pii/S0166516213002760

745 Politi Y., Arad T., Klein E., Weiner S. and Addadi L. (2009) Sea Urchin Spine CalciteForms via a
746 Transient Amorphous Calcium Carbonate Phase. *Science* **306**, 1161–1164. Available at:
747 http://www.ncbi.nlm.nih.gov/pubmed/15539597.

748 Postma D. (1980) Formation of siderite and vivianite and the pore-water composition of a Recent
749 bog sediment in Denmark. *Chem. Geol.* **31**, 225–244.

750 Pye K., Dickson J. A. D., Schiavon N., Coleman M. L. and Cox M. (1990) Formation of siderite-Mg-
751 calcite-iron sulphide concretions in intertidal marsh and sandflat sediments, north Norfolk,
752 England. *Sedimentology* **37**, 325–343.

753 Rakovan J. and Reeder R. J. (1996) Intracrystalline rare earth element distributions in apatite:
754 Surface structural influences on incorporation during growth. *Geochim. Cosmochim. Acta* **60**,
755 4435–4445. Available at:
756 https://www.sciencedirect.com/science/article/pii/S001670379600244X

757 Reeder R. J. (1983) Crystal chemistry of the rhombohedral carbonates. *Rev. Mineral. Geochemistry*
758 **11**, 1–47.

759 Reeder R. J. (1996) Interaction of divalent cobalt, zinc, cadmium, and barium with the calcite
760 surface during layer growth. *Geochim. Cosmochim. Acta* **60**, 1543–1552. Available at:
761 https://www.sciencedirect.com/science/article/pii/0016703796000348

762 Reeder R. J., Fagioli R. O. and Meyers W. J. (1990) Oscillatory zoning of Mn in solution-grown
763 calcite crystals. *Earth-Science Rev.* **29**, 39–46. Available at:

https://www.sciencedirect.com/science/article/pii/001282529090026R

Reeder R. J. and Rakovan J. (1999) Surface Structural Controls on Trace Element Incorporation during Crystal Growth. In *Growth, Dissolution and Pattern Formation in Geosystems* (eds. B. Jamtveit and P. Meakin). Springer Netherlands, Dordrecht. pp. 143–162. Available at: https://doi.org/10.1007/978-94-015-9179-9_6.

Rimstidt J. D., Balog A. and Webb J. (1998) Distribution of trace elements between carbonate minerals and aqueous solutions. *Geochim. Cosmochim. Acta* **62**, 1851–1863. Available at: https://www.sciencedirect.com/science/article/pii/S0016703798001252

Robinson S. A., Scotchman J. I., White T. S. and Atkinson T. C. (2010) Constraints on palaeoenvironments in the Lower Cretaceous Wealden of southern England, from the geochemistry of sphaerosiderites. *J. Geol. Soc. London.* **167**, 303–311.

Rodriguez-Navarro C., Burgos Cara A., Elert K., Putnis C. V. and Ruiz-Agudo E. (2016) Direct Nanoscale Imaging Reveals the Growth of Calcite Crystals via Amorphous Nanoparticles. *Cryst. Growth Des.* **16**, 1850–1860.

Romanek C. S., Jiménez-López C., Navarro A. R., Sánchez-Román M., Sahai N. and Coleman M. (2009) Inorganic synthesis of Fe-Ca-Mg carbonates at low temperature. *Geochim. Cosmochim. Acta* **73**, 5361–5376.

Sel O., Radha A. V., Dideriksen K. and Navrotsky A. (2012) Amorphous iron (II) carbonate: Crystallization energetics and comparison to other carbonate minerals related to CO2 sequestration. *Geochim. Cosmochim. Acta* **87**, 61–68. Available at: https://www.sciencedirect.com/science/article/pii/S0016703712001536

Steefel C. I. and Van Cappellen P. (1990) A new kinetic approach to modeling water-rock interaction: The role of nucleation, precursors, and Ostwald ripening. *Geochim. Cosmochim.*

Acta **54**, 2657–2677. Available at: https://www.sciencedirect.com/science/article/pii/0016703790900034

Steinmann P. and Shotyk W. (1997) Chemical composition, pH, and redox state of sulfur and iron in complete vertical porewater profiles from two Sphagnum peat bogs, Jura Mountains, Switzerland. *Geochim. Cosmochim. Acta* **61**, 1143–1163.

Stephenson A., DeYoreo J., Wu L., Wu K., Hoyer J. and Dove P. (2008) Peptides Enhance Magnesium Origins of Vital Effects. *Science (80-.).* **322**, 724–727.

Suarez M. B., González L. A., Ludvigson G. A., Vega F. J. and Alvarado-Ortega J. (2009) Isotopic composition of low-latitude paleoprecipitation during the Early Cretaceous. *Geol. Soc. Am. Bull.* **121**, 1584–1595. Available at: https://pubs.geoscienceworld.org/gsabulletin/article/121/11-12/1584-1595/2350

Sunagawa I. (2007) *Crystals : Growth, morphology, and perfection*., Cambridge University Press.

Teng H. H., Dove P. M. and De Yoreo J. J. (2000) Review on MAC Protocols for Underwater Acoustic Networks. *Geochemica Cosmochem. Acta* **64**, 2255–2266. Available at: https://irjet.net/archives/V4/i1/IRJET-V4I1310.pdf.

Thornber M. R. and Nickel E. H. (1976) Supergene alteration of sulphides. III. The composition of associated carbonates. *Chem. Geol.* **17**, 45–72. Available at: https://www.sciencedirect.com/science/article/pii/0009254176900218

Ufnar D. F., Gonzalez L. A., Ludvigson G. A., Brenner R. L. and Witzkes B. J. (2004a) Diagenetic overprinting of the sphaerosiderite palaeoclimate proxy: Are records of pedogenic groundwater ??18O values preserved? *Sedimentology* **51**, 127–144.

Ufnar D. F., Ludvigson G. A., González L. A., Brenner R. L. and Witzke B. J. (2004b) High latitude meteoric δ18O compositions: Paleosol siderite in the Middle Cretaceous Nanushuk Formation,

North Slope, Alaska. *Geol. Soc. Am. Bull.* **116**, 463. Available at: https://pubs.geoscienceworld.org/gsabulletin/article/116/3-4/463-473/2072

Wang D., Wallace A. F., De Yoreo J. J. and Dove P. M. (2009) Carboxylated molecules regulate magnesium content of amorphous calcium carbonates during calcification. *Proc. Natl. Acad. Sci.* **106**, 21511–21516.

Wang Y. and Merino E. (1992) Dynamic model of oscillatory zoning of trace elements in calcite: Double layer, inhibition, and self-organization. *Geochim. Cosmochim. Acta* **56**, 587–596. Available at: https://www.sciencedirect.com/science/article/pii/001670379290083U

Weibel R., Lindstr??m S., Pedersen G. K., Johansson L., Dybkj??r K., Whitehouse M. J., Boyce A. J. and Leng M. J. (2016) Groundwater table fluctuations recorded in zonation of microbial siderites from end-Triassic strata. *Sediment. Geol.* **342**, 45–65. Available at: http://dx.doi.org/10.1016/j.sedgeo.2016.06.009.

Weiner S. and Dove P. M. (2003) An Overview of Biomineralization Processes and the Problem of the Vital Effect. *Rev. Mineral. Geochemistry* **54**, 1–29. Available at: https://pubs.geoscienceworld.org/rimg/article/54/1/1-29/87485

Weiss I. M., Tuross N., Addadi L. and Weiner S. (2002) Mollusc larval shell formation: Amorphous calcium carbonate is a precursor phase for aragonite. *J. Exp. Zool.* **293**, 478–491.

Zhang Y. and Dawe R. A. (2000) Influence of Mg2+ on the kinetics of calcite precipitation and calcite crystal morphology. *Chem. Geol.* **163**, 129–138. Available at: http://www.sciencedirect.com/science/article/pii/S0009254199000972.